Icing diagnosis in unmanned aerial vehicles using an LPV multiple model estimator ⋆

Damiano Rotondo[1], **Andrea Cristofaro**[2], **Vahid Hassani**[3], **Tor Arne Johansen**[1]

[1] *Center for Autonomous Marine Operations and Systems, Department of Engineering Cybernetics, Norwegian University of Science and Technology, 7491 Trondheim, Norway.*

[2] *School of Science and Technology, University of Camerino, 62302 Camerino, Italy.*

[3] *Department of Marine Technology, Norwegian University of Science and Technology, 7491 Trondheim, Norway.*

Abstract: The phenomenon of icing, i.e. ice accretion on aircraft surfaces, affects the flight performance of unmanned aerial vehicles (UAVs). Autonomous icing detection schemes are needed in order to assure high efficiency and limit energy consumption of de-icing and anti-icing schemes. The novel contribution of this paper is to apply a linear parameter varying multiple model adaptive estimator to the model of the longitudinal nonlinear dynamics of a UAV, in order to achieve an icing diagnosis that provides information about the icing location. An advantage of applying a linear parameter varying approach is that the icing diagnosis scheme is consistent with the UAV dynamics for a wide range of operating conditions, and it uses only existing standard sensors. Simulation results are used to illustrate the application of the proposed method.

Keywords: Multiple models; linear parameter varying; unmanned aerial vehicles; icing diagnosis.

1. INTRODUCTION

The phenomenon of icing, i.e. ice accretion on aircraft surfaces, is a recognized problem in aviation (Caliskan and Hajijev, 2013). The formation of ice layers decreases significantly the lift and the manoeuvrability of unmanned aerial vehicles (UAVs), while simultaneously increasing drag, weight and power consumption (Gent et al., 2000). Icing is a common cause for UAV incidents, which impedes conducting UAV operations in environments that present potential icing conditions (Gober et al., 2001).

With the aim of mitigating the effect of icing, some ice protection systems (IPS) have been proposed recently. For example, Sørensen et al. (2015b) have proposed an electrically conductive carbon nano material based coating for temperature control of UAV airfoil surfaces. This solution allows increasing rapidly the airfoil surface temperature (de-icing) and maintaining it at an approximately constant value above the freezing point (anti-icing), when needed.

However, in order to assure high efficiency and limit energy consumption, icing detection schemes are needed. Recently, several approaches have been proposed to achieve this goal, such as unknown input observers (UIOs) (Tousi and Khorasani, 2011, Rotondo et al., 2015a, 2016) and statistical methods (Sørensen et al., 2015a).

The above mentioned approaches are interesting, but share a common limitation, which is to be able to perform icing detection, i.e. assessing whether icing has occurred or not, but without providing any information about the icing severity factor (ISF) or the location of icing, i.e. whether it is affecting the wings, the tail, or all the UAV. Concerning the ISF, Seron et al. (2015) and Cristofaro et al. (2015) have suggested to employ a bank of observers, each of which corresponds to a quantised value of the ISF, and estimation algorithms that take into account the values taken by suitable signals have been also proposed (Wenz and Johansen, 2016). However, obtaining a detailed icing diagnosis, comprising information about the icing location, is still an open problem.

Recently, a linear parameter varying (LPV) multiple model adaptive estimator (MMAE) has been proposed for estimating the state and the value of unknown parameters in discrete time uncertain LPV plants (Rotondo et al., 2017). The proposed LPV MMAE comprises a collection of local observers, each of which provides the state estimation which would correspond to a predefined value of the unknown parameters. Under some conditions, the identified unknown parameters correspond to the observer that exhibits the smallest output prediction error energy.

In this regard, the novel contribution of this paper is to apply the LPV MMAE to the model of the longitudinal nonlinear dynamics of a UAV, in order to achieve an icing diagnosis that provides information about the icing location. Unlike linearisation techniques, the LPV formulation does not involve any approximation, since it relies on an exact transformation of the original non-linear system into a linear-like one (Shamma, 2012). Hence, an advantage of the proposed LPV MMAE-

⋆ D. Rotondo acknowledges that this work was carried out during the tenure of an ERCIM Alain Bensoussan Fellowship Programme. This work was also supported by the Research Council of Norway through the Centers of Excellence funding scheme, Project number 223254 - Centre for Autonomous Marine Operations and Systems (NTNU-AMOS). e-mail: damiano.rotondo@yahoo.it

based icing diagnosis scheme is to be consistent with the UAV dynamics for a wide range of operating conditions.

The paper is structured as follows. Section 2 presents the quasi-LPV model of the longitudinal equations of motion of a UAV and how icing affects them. Section 3 describes the LPV MMAE and its relevant properties. The case study and the simulation results are discussed in Section 4. Finally, Section 5 outlines the main conclusions.

2. QUASI-LPV MODEL OF THE UAV SUBJECT TO ICING

Following Rotondo et al. (2015a), the longitudinal equations of motion of a UAV (Beard and McLain, 2012), under low-angle-of-attack condition, can be brought to a quasi-LPV form using the non-linear embedding in the parameters approach (Kwiatkowski et al., 2006, Rotondo et al., 2015b), as follows (see Table 1 for a description of the symbols):

$$\dot{x} = A(u,w,q,\theta)x + B(u,w)\upsilon + G(\theta)\omega + d(\theta) \tag{1}$$

where $x = (u,w,q,\theta)^T$ is the state vector, $\upsilon = (\delta_t^2, \delta_e)^T$ is the input vector, $\omega = (\dot{\omega}_x, \dot{\omega}_z)^T$ is a disturbance vector that represents the wind effect, and the matrices $A(u,w,q,\theta)$, $B(u,w)$, $G(\theta)$ and $d(\theta)$ are given by:

$$A(u,w,q,\theta) = \begin{pmatrix} a_{11}(\cdot) & a_{12}(\cdot) & a_{13}(\cdot) & 0 \\ a_{21}(\cdot) & a_{22}(\cdot) & a_{23}(\cdot) & 0 \\ a_{31}(\cdot) & a_{32}(\cdot) & a_{33}(\cdot) & 0 \\ 0 & 0 & 1 & 0 \end{pmatrix} \tag{2}$$

$$B(u,w) = \begin{pmatrix} b_{11} & b_{12}(\cdot) \\ 0 & b_{22}(\cdot) \\ 0 & b_{32}(\cdot) \\ 0 & 0 \end{pmatrix} \quad d(\theta) = \begin{pmatrix} -g\sin\theta \\ g\cos\theta \\ 0 \\ 0 \end{pmatrix} \tag{3}$$

$$G(\theta) = \begin{pmatrix} -\cos\theta & -\sin\theta \\ -\sin\theta & \cos\theta \\ 0 & 0 \\ 0 & 0 \end{pmatrix} \tag{4}$$

where:

$$a_{11}(\cdot) = \frac{\rho u S}{2m}\left[(C_{L_0} + C_{L_\alpha}\alpha)\sin\alpha - (C_{D_0} + C_{D_\alpha}\alpha)\cos\alpha - \frac{S_{prop}C_{prop}}{S}\right]$$

$$a_{12}(\cdot) = \frac{\rho w S}{2m}\left[(C_{L_0} + C_{L_\alpha}\alpha)\sin\alpha - (C_{D_0} + C_{D_\alpha}\alpha)\cos\alpha - \frac{S_{prop}C_{prop}}{S}\right]$$

$$a_{13}(\cdot) = -w + \frac{\rho S c V_a}{4m}\left(C_{L_q}\sin\alpha - C_{D_q}\cos\alpha\right)$$

$$a_{21}(\cdot) = -\frac{\rho u S}{2m}\left[(C_{D_0} + C_{D_\alpha}\alpha)\sin\alpha + (C_{L_0} + C_{L_\alpha}\alpha)\cos\alpha\right]$$

$$a_{22}(\cdot) = -\frac{\rho w S}{2m}\left[(C_{D_0} + C_{D_\alpha}\alpha)\sin\alpha + (C_{L_0} + C_{L_\alpha}\alpha)\cos\alpha\right]$$

$$a_{23}(\cdot) = u - \frac{\rho S c V_a}{4m}\left(C_{D_q}\sin\alpha + C_{L_q}\cos\alpha\right)$$

$$a_{31}(\cdot) = \frac{\rho S c u}{2J_y}\left(C_{m_0} + C_{m_\alpha}\alpha\right)$$

$$a_{32}(\cdot) = \frac{\rho S c w}{2J_y}\left(C_{m_0} + C_{m_\alpha}\alpha\right)$$

$$a_{33}(\cdot) = \frac{\rho V_a S c^2}{4J_y} C_{m_q}$$

$$b_{11} = \frac{\rho S_{prop} C_{prop}}{2m} k_m^2$$

$$b_{12}(\cdot) = \frac{\rho S V_a^2}{2m}\left(C_{L_{\delta_e}}\sin\alpha - C_{D_{\delta_e}}\cos\alpha\right)$$

$$b_{22}(\cdot) = -\frac{\rho V_a^2 S}{2m}\left(C_{D_{\delta_e}}\sin\alpha + C_{L_{\delta_e}}\cos\alpha\right)$$

$$b_{32}(\cdot) = \frac{\rho V_a^2 S c}{2J_y} C_{m_{\delta_e}}$$

Table 1. Symbols description

Symbol	Description
u	Horizontal velocity relative to the wind
w	Vertical velocity relative to the wind
q	Pitch rate
θ	Pitch angle
δ_t	Throttle deflection
δ_e	Elevator efficiency
$\dot{\omega}_x$	Horizontal wind acceleration
$\dot{\omega}_z$	Vertical wind acceleration
g	Gravitational acceleration
ρ	Air density
S	Wing surface area
m	Airframe mass
α	Angle-of-attack
c	Mean aerodynamic chord of the wing
S_{prop}	Area of the propeller
k_m	Efficiency of the motor
J_y	Element of the inertia matrix
V_a	Airspeed with respect to the mass
C_i	Stability and control derivatives

2.1 Icing effects

The accretion of ice on the UAV surfaces modifies the stability and control derivatives according to the following linear model (Bragg et al., 2002):

$$C_i^* = (1 + \eta K_i) C_i \tag{5}$$

where η is the ISF and the coefficients K_i depend on the UAV design and atmospheric conditions. The clean condition corresponds to $\eta = 0$, while the most severe icing condition occurs for $\eta = 0.2$.

Table 2 lists the coefficients used in this work, for different icing configurations: wing icing, tail icing and full icing. It is worth remarking that these coefficients have been computed by mimicking the proportional variation of the stability and control derivatives for a Twin Otter aircraft (Bragg et al., 2002), and they are expected to differ in the case of other UAVs. These values are used in the simulator in order to provide realistic icing effects. However, when applying the proposed LPV MMAE strategy to a real UAV, it would be of paramount importance to identify properly the values of these coefficients for the specific UAV.

It is evident that the effect of icing on the quasi-LPV model (1)-(4) involves a modification of the matrices $A(u,w,q,\theta)$ and $B(u,w)$, which take different values according to the presence and type of icing. Hence, (1) can be rewritten more generally as:

$$\dot{x} = A_\kappa(u,w,q,\theta)x + B_\kappa(u,w)\upsilon + G(\theta)\omega + d(\theta) \tag{6}$$

where the index κ is an icing indicator, such that $\kappa = 1$ corresponds to a clean UAV (no icing), $\kappa = 2$ corresponds to full icing, $\kappa = 3$ to wing icing and $\kappa = 4$ to tail icing.

As a matter of example, the element $a_{31}^{tail}(\cdot)$ of $A_3(u,w,q,\theta)$ would be:

$$a_{31}^{tail}(\cdot) = \frac{\rho S c u}{2J_y}\left(C_{m_0} + (1 + \eta K_{m\alpha}^{tail}) C_{m_\alpha}\alpha\right) \tag{7}$$

3. LPV MULTIPLE MODEL ADAPTIVE ESTIMATOR

Let us consider a discrete time multiple input multiple output (MIMO) LPV model of the form:

Table 2. Coefficients K_i for different icing configurations

	K_{L_α}	K_{L_q}	$K_{L_{\delta_e}}$	K_{D_0}
wing icing	-0.2809	-0.0675	-0.1151	1.0976
tail icing	-0.1237	-0.0675	-0.3536	0.6098
full icing	-0.5000	-0.0675	-0.4770	2.5610
	K_{m_α}	K_{m_q}	$K_{m_{\delta_e}}$	
wing icing	-0.0954	-0.1755	-0.0891	
tail icing	-0.1794	-0.1755	-0.4224	
full icing	-0.4962	-0.1755	-0.5000	

$$x(t+1) = A_\kappa(\vartheta(t))x(t) + B_\kappa(\vartheta(t))\upsilon(t) + G_\kappa(\vartheta(t))\omega(t) + d(\vartheta(t)) \quad (8)$$

$$y(t) = C_\kappa(\vartheta(t))x(t) + v(t) \quad (9)$$

where $x \in \mathbb{R}^n$ denotes the state vector, $\upsilon \in \mathbb{R}^m$ is the control input vector, $\omega \in \mathbb{R}^r$ is a disturbance vector that cannot be measured, $d \in \mathbb{R}^n$ is a known additive term, and $y \in \mathbb{R}^q$ is the measured output vector, which is affected by the measurement noise $v \in \mathbb{R}^q$. The initial condition $x(0)$ is assumed to be unknown, while the signals $\omega(t), v(t)$ are uncorrelated and may be described as white noises with covariance matrices S_ω and S_v, respectively. The matrix functions $A_\kappa(\vartheta(t))$, $B_\kappa(\vartheta(t))$, $C_\kappa(\vartheta(t))$ and $G_\kappa(\vartheta(t))$ depend on both an *unknown parameter* κ and a *known time-varying parameter vector* $\vartheta \in \Theta \subset \mathbb{R}^s$, being Θ a known bounded set.

In order to estimate the state, a finite set of candidate parameter values $\{\kappa_1, \ldots, \kappa_N\}$ indexed by $i \in \{1, \ldots, N\}$ are considered. Notice that the quasi-LPV model of the UAV subject to icing described in Section 2 (see Eq. (6)) can be represented in the form (8) by applying a discretization method, e.g. Euler or Runge-Kutta, with $N = 4$ as detailed in Section 2.1.

It is assumed that for each candidate parameter value κ_i, $i \in \{1, \ldots, N\}$, the corresponding matrix functions $A_{\kappa_i}(\vartheta(t))$, $B_{\kappa_i}(\vartheta(t))$, $C_{\kappa_i}(\vartheta_t)$ and $G_{\kappa_i}(\vartheta_t)$ can be described as the convex sum of $L \geq 1$ constant matrices denoted as *vertex matrices*:

$$\begin{pmatrix} A_{\kappa_i}(\vartheta(t)) & B_{\kappa_i}(\vartheta(t)) \\ C_{\kappa_i}(\vartheta(t)) & G_{\kappa_i}(\vartheta(t)) \end{pmatrix} = \sum_{j=1}^{L} h_i^{(j)}(\vartheta(t)) \begin{pmatrix} A_{\kappa_i}^{(j)} & B_{\kappa_i}^{(j)} \\ C_{\kappa_i}^{(j)} & G_{\kappa_i}^{(j)} \end{pmatrix} \quad (10)$$

where, for a given i, the coefficients $h_i^{(j)}(\vartheta(t))$ satisfy the following property:

$$\sum_{j=1}^{L} h_i^{(j)}(\vartheta) = 1, \quad h_i^{(j)}(\vartheta) \in [0,1] \quad \forall \vartheta \in \Theta \quad (11)$$

In Rotondo et al. (2017), taking into account previous results developed in Hassani et al. (2009), the following LPV MMAE has been proposed:

$$\hat{x}(t) = \sum_{i=1}^{N} p_i(t)\hat{x}(t|\kappa_i) \quad (12)$$

$$\hat{y}(t) = \sum_{i=1}^{N} p_i(t)\hat{y}(t|\kappa_i) \quad (13)$$

$$\hat{\kappa}(t) = \kappa_{i^*(t)}, \quad i^*(t) = \arg\max_{i \in \{1,\ldots,N\}} p_i(t) \quad (14)$$

where $\hat{x}(t)$, $\hat{y}(t)$ and $\hat{\kappa}(t)$ are the estimates of the state $x(t)$, the output $y(t)$, and the unknown parameter κ, respectively, $\hat{x}(t|\kappa_i)$, $\hat{y}(t|\kappa_i)$ correspond to *local* state estimations, and $p_i(t)$ are the dynamic weights, generated as follows:

$$p_i(t+1) = \frac{p_i(t)\beta_i(t)e^{-\psi_i(t)}}{\sum_{j=1}^{N} p_j(t)\beta_j(t)e^{-\psi_j(t)}} \quad (15)$$

where $\beta_i(t)$ is a positive weighting function and $\psi_i(t)$ is the *error measuring function*, which maps the measurable signals and the local state estimation $\hat{x}(t|\kappa_i)$ to a nonnegative real value.

Following Rotondo et al. (2017), $\psi_i(t)$ and $\beta_i(t)$ are chosen as:

$$\psi_i(t) = \frac{1}{2}\|y(t) - \hat{y}(t|\kappa_i)\|^2_{S_{\kappa_i}(\vartheta(t))^{-1}} \quad (16)$$

$$\beta_i(t) = \frac{1}{\sqrt{|S_{\kappa_i}(\vartheta(t))|}} \quad (17)$$

where $S_{\kappa_i}(\vartheta(t))$ is a positive definite weighting matrix function, which scales the energy of the estimation error sequences making them comparable, and $\|x\|_S = \sqrt{x^T S x}$.

In (12)-(13), the local estimations $\hat{x}(t|\kappa_i)$, $\hat{y}(t|\kappa_i)$ are obtained through the following LPV Kalman filter (Simon, 2003):

$$\hat{x}(t|\kappa_i) = \sum_{j=1}^{L} \hat{x}_j(t|\kappa_i) \quad (18)$$

$$\hat{y}(t|\kappa_i) = C_{\kappa_i}(\vartheta(t))\hat{x}(t|\kappa_i) \quad (19)$$

where $\hat{x}_j(t|\kappa_i)$, $j \in \{1, \ldots, L\}$ are obtained as follows:

$$\hat{x}_j(t|\kappa_i) = \left[I - K_{\kappa_i}^{(j)} C_{\kappa_i}^{(j)}\right] \hat{x}_j^-(t|\kappa_i) + K_{\kappa_i}^{(j)} h_i^{(j)}(\vartheta(t)) y(t) \quad (20)$$

$$\hat{x}_j^-(t+1|\kappa_i) = A_{\kappa_i}^{(j)} \hat{x}_j(t|\kappa_i) + h_i^{(j)}(\vartheta(t)) \left(B_{\kappa_i}^{(j)} \upsilon(t) + d(t)\right) \quad (21)$$

with:

$$K_{\kappa_i}^{(j)} = P_{\kappa_i}^{(j)} \left(C_{\kappa_i}^{(j)}\right)^T \left[C_{\kappa_i}^{(j)} P_{\kappa_i}^{(j)} \left(C_{\kappa_i}^{(j)}\right)^T + S_v\right]^{-1} \quad (22)$$

where $P_{\kappa_i}^{(j)}$ is the solution of the discrete Riccati equation:

$$P_{\kappa_i}^{(j)} = A_{\kappa_i}^{(j)} \left[P_{\kappa_i}^{(j)} - K_{\kappa_i}^{(j)} C_{\kappa_i}^{(j)} P_{\kappa_i}^{(j)}\right] \left(A_{\kappa_i}^{(j)}\right)^T + G_{\kappa_i}^{(j)} S_\omega \left(G_{\kappa_i}^{(j)}\right)^T \quad (23)$$

and the superscript $-$ indicates that the quantity is calculated before the measurement is taken into account.

In Rotondo et al. (2017), it has been suggested that a possible choice for $S_{\kappa_i}(\vartheta(t))$ in (16)-(17) could be:

$$S_{\kappa_i}(\vartheta(t)) = \sum_{j=1}^{L} h_i^{(j)}(\vartheta(t)) S_{\kappa_i}^{(j)} \quad (24)$$

with:

$$S_{\kappa_i}^{(j)} = C_{\kappa_i}^{(j)} P_{\kappa_i}^{(j)} \left(C_{\kappa_i}^{(j)}\right)^T + S_v \quad (25)$$

3.1 Properties of the LPV MMAE

Hereafter, the relevant properties of the proposed LPV MMAE are summarized. The proofs of these properties can be found in Rotondo et al. (2017).

The following property shows positiveness and boundedness of the dynamic weights $p_i(t)$.

Property 1. Assume that $p_i(0) > 0 \ \forall i \in \{1, \ldots, N\}$. Then, all the signals $p_i(t)$ generated by (15) are nonnegative, uniformly bounded and contained in $(0, 1)$, with:

$$\sum_{i=1}^{N} p_i(t) = 1 \qquad \forall t > 0 \quad (26)$$

Table 3. System parameters values

Param.	Value	Param.	Value	Param.	Value
m	$1.56\,kg$	C_{L_0}	0.09167	C_{D_q}	0
J_y	$0.0576\,kg\,m^2$	C_{D_0}	0.01631	C_{m_q}	-1.3990
S	$0.2589\,m^2$	C_{m_0}	-0.02338	$C_{L_{\delta_e}}$	0.2724
c	$0.3302\,m$	C_{L_α}	3.5016	$C_{D_{\delta_e}}$	0.3045
S_{prop}	$0.0314\,m^2$	C_{D_α}	0.2108	$C_{m_{\delta_e}}$	-0.3254
ρ	$1.2682\,kg/m^3$	C_{m_α}	-0.5675	C_{prop}	1.0
k_m	20	C_{L_q}	2.8932		

On the other hand, the following property shows that the dynamic weights $p_i(t)$ exhibit convergence if some conditions are fulfilled.

Property 2. Let $i^* \in \{1,\dots,N\}$ be an index for the set of candidate parameter values $\{\kappa_1,\dots,\kappa_N\}$, and let $\mathscr{I} = \{1,\dots,N\}\backslash i^*$ be an index set. Suppose there exist positive constants n_1, t_1, ε and ε_1 such that the following conditions hold for all $t \geq t_1$ and $n \geq n_1$:

$$\frac{1}{n}\sum_{\tau=t}^{t+n-1}(\psi_{i^*}(\tau)+\varepsilon) < \frac{1}{n}\sum_{\tau=t}^{t+n-1}\min_{j\in\mathscr{I}}\psi_j(\tau) \tag{27}$$

$$\ln\bar{\beta}(t) - \ln\beta_{i^*}(t) < \varepsilon_1 < \varepsilon \tag{28}$$

where:

$$\bar{\beta}(t) = \max_{j\in\mathscr{I}}\beta_j(t) \tag{29}$$

Then $p_{i^*}(t)$ calculated as in (15) satisfies $p_{i^*}(t) \to 1$ as $t \to \infty$.

The following property provides additional information about the parameter estimate $\hat{\kappa}(t)$ given by (14).

Property 3. Assume that the conditions of Property 2 hold, and let $\psi_i(t)$ be defined as in (16). Then, the parameter estimate $\hat{\kappa}(t)$ converges to the closest κ_i as $t \to \infty$ in the following sense:

$$\lim_{t\to\infty}\hat{\kappa}(t) = \kappa_{i^*} \tag{30}$$

$$i^* = \arg\min_{i\in\{1,\dots,N\}}\lim_{n\to\infty}\frac{1}{n}\sum_{\tau=t}^{t+n-1}\psi_i(\tau) \qquad \forall t \geq t_1 \tag{31}$$

4. CASE STUDY

Let us consider the case study of a small UAV, with the parameters appearing in the quasi-LPV model described in Section 2 taken from Beard and McLain (2012) and resumed in Table 3. The UAV is controlled by an autopilot, which is responsible to make the UAV track some desired reference longitudinal velocity and pitch angle. For the considered simulation, the following reference signals are used:

$$u_{ref}(t) = \begin{cases} 22 & t < 50s \\ (4550-3t)/200 & 50s \leq t < 250s \\ (3550+2t)/200 & 250s \leq t < 450s \\ 21 & t \geq 450s \end{cases}$$

$$\theta_{ref}(t) = \begin{cases} \pi/15 & t < 100s \\ (t+100\pi-100)/1500 & 100s \leq t < 250s \\ (100\pi+400-t)/1500 & 250s \leq t < 400s \\ \pi/15 & t \geq 400s \end{cases}$$

and the initial state is set as $x(0) = (18,3,0,\pi/15)^T$. The initial condition for the dynamic weight is chosen as $p(0) = (0.25,0.25,0.25,0.25)^T$.

It is assumed that the whole state is available for measurement, i.e. $C_\kappa(\theta(t)) = I$. The measurement noise $v(t)$ is generated as a white noise with covariance $S_v = diag([0.1,0.1,10^{-6},10^{-6}])$. On the other hand, the wind disturbance $\omega(t)$ is generated using the Dryden wind turbulence model provided by the Aerospace Toolbox of Matlab, with a light probability (10^{-2}) of exceeding the high-altitude turbulence intensity. However, for calculating the solution of the discrete Riccati equation (23), a value $S_\omega = diag([0.8,0.8])$ is used.

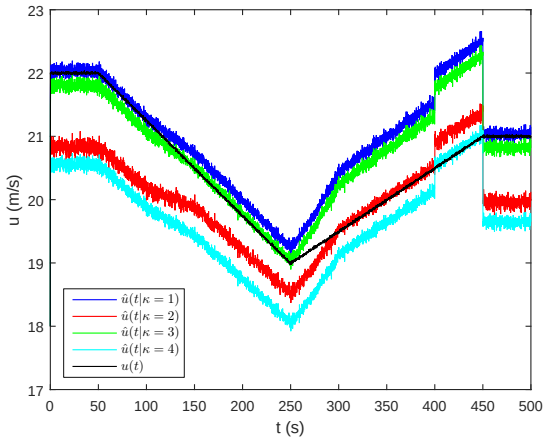

Fig. 1. Horizontal velocity u and its estimations.

By applying an Euler discretization with sampling period $T_s = 0.01\,s$, and a *bounding box method* (Sun and Postlethwaite, 1998), the quasi-LPV model of the UAV subject to icing (1) has been brought to the form (10) by considering the following limits on the state variables: $u \in [15,25]$, $w \in [0.3,3]$, $q \in [-0.04,0.04]$ and $\theta \in [-0.35,0.35]$.

The considered fault scenario comprises all possible icing configurations, for which a value $\eta = 0.2$ is used. From $t = 0\,s$ to $t = 100\,s$, the UAV works under nominal conditions ($\kappa = 1$). At time $t = 100\,s$, an ice layer builds incrementally on the wings, such that the UAV operates under wing icing conditions ($\kappa = 3$) from $t = 150\,s$ to $t = 250\,s$. At time $t = 250\,s$, another ice layer builds incrementally on the tail such that full icing conditions ($\kappa = 2$) are considered from $t = 300\,s$ to $t = 400\,s$. At time $t = 400\,s$, a de-icing system is applied to the wings, such that the icing condition changes abruptly to tail icing ($\kappa = 4$). Finally, at time $t = 450\,s$, also the tail is de-iced, and the UAV returns to the clean state ($\kappa = 1$).

Figs. 1-4 show the responses of the state variables obtained from the simulation, along with their estimations $\hat{x}(t|\kappa_i)$ given by (18). Moreover, Fig. 5 compares the estimation of the angle-of-attack α calculated using the estimations available for u and w with its real value $\alpha = \arctan(w/u)$. It can be seen that the state variables that are affected the most by icing are the horizontal and vertical velocity, respectively. Also, aside from the smooth transitions in the time intervals $[100\,s,150\,s]$ and $[250\,s,300\,s]$, the estimations that better fit the real value of the state is the one corresponding to the icing conditions of the system. For example, up to $t = 100\,s$, $\hat{u}(t|\kappa = 1)$ (no icing) is the signal that fits better $u(t)$. On the other hand, in the time interval $t \in [150\,s,250\,s]$ the icing phenomenon affects the wings ($\kappa = 3$), and the estimation that fits better $u(t)$ is $\hat{u}(t|\kappa = 3)$.

Fig. 6 shows the obtained error measuring functions $\psi_i(t)$ (notice that solid lines are added in order to show smoothed version of the signals for graphical purposes), whereas Fig. 7 shows a zoom on the time interval $[399\,s,401\,s]$. The corresponding dynamic weights $p_i(t)$ are shown in Fig. 8. Then, using the

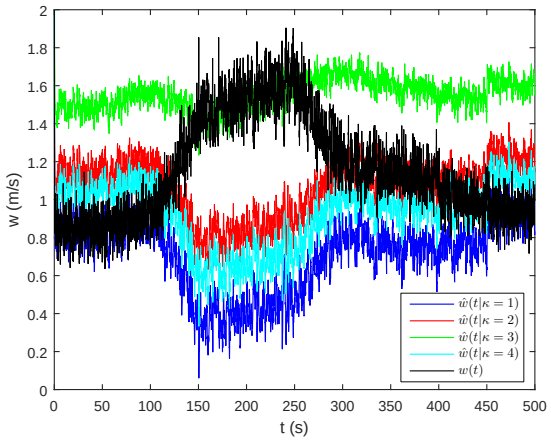

Fig. 2. Vertical velocity w and its estimations.

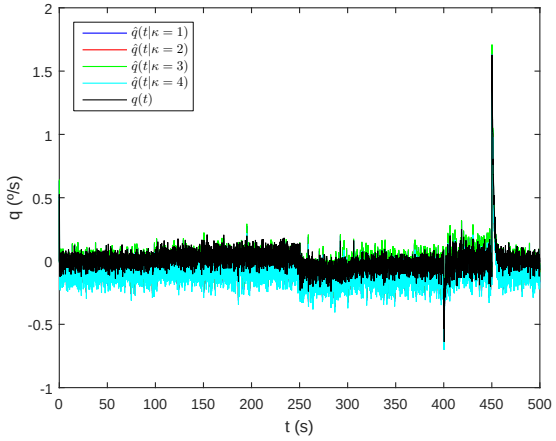

Fig. 3. Pitch rate q and its estimations.

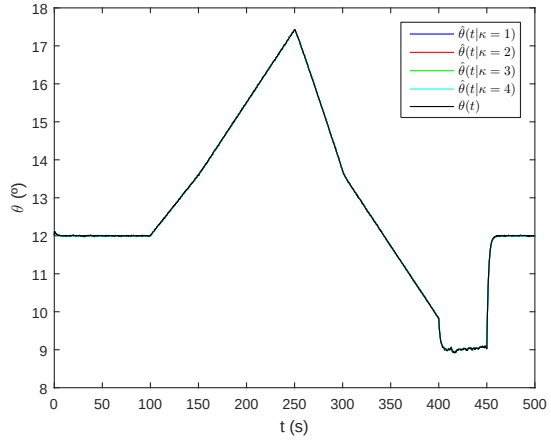

Fig. 4. Pitch angle θ and its estimations.

estimator (14), the icing diagnosis can be performed. At the beginning of the simulation, $\hat{\kappa}=1$ (no icing) holds. At time $t=128.45\,s$, the presence of wing icing ($\hat{\kappa}=3$) is correctly diagnosed. Full icing ($\hat{\kappa}=2$) and tail icing ($\hat{\kappa}=4$) are diagnosed at time $t=277.04\,s$ and time $t=401.16\,s$, respectively. Finally, the situation of no icing is correctly diagnosed at time $t=450.41\,s$.

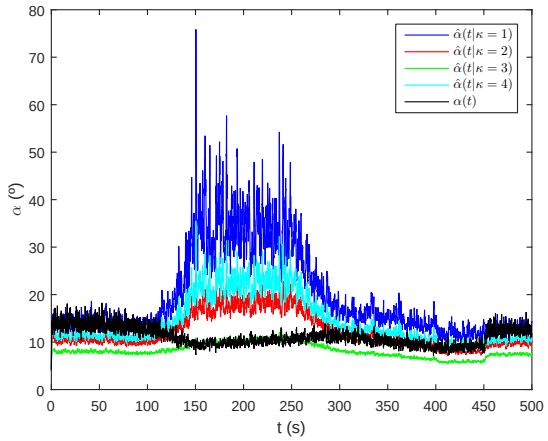

Fig. 5. Angle-of-attack α and its estimations.

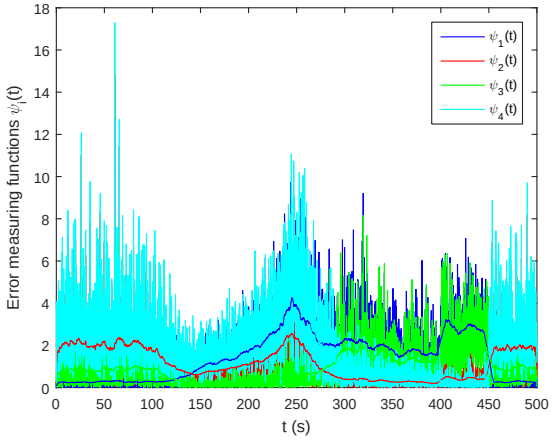

Fig. 6. Error measuring functions $\psi_i(t)$.

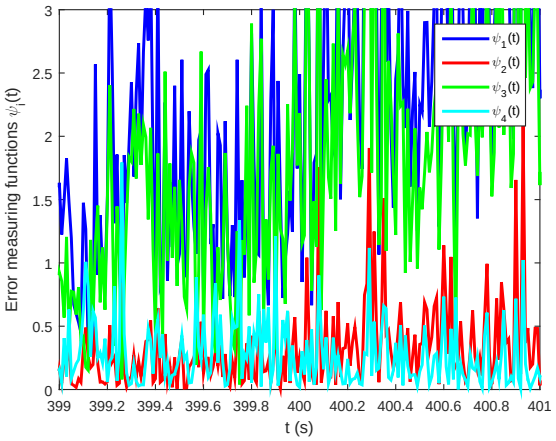

Fig. 7. Error measuring functions $\psi_i(t)$ (zoom).

5. CONCLUSIONS

This paper has proposed a method for icing diagnosis in UAVs using a linear parameter varying multiple model adaptive estimator. The linear parameter varying multiple model adaptive estimator comprises a collection of observers, each of which provides the state estimation which would correspond to a predefined value of the unknown parameter (the icing condi-

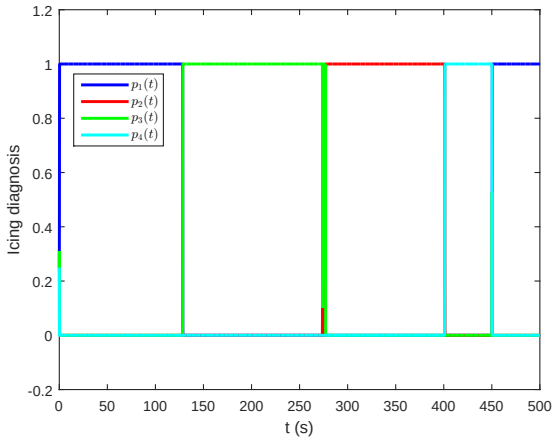

Fig. 8. Dynamic weights $p_i(t)$.

tion). Under some suitable conditions, the identified unknown parameter corresponds to the observer that exhibits the smallest output prediction error energy. An advantage of the proposed approach is that the provided information is not limited to icing detection, i.e. assessing whether icing has occurred or not, but also comprises icing location (whether icing affects the wings, the tail or all of the UAV). The case study of a small UAV has allowed validating the effectiveness of the proposed technique in simulation.

Future work will aim at applying the proposed icing diagnosis strategy to an experimental setup. In order to do so, it is of paramount importance to further develop the linear parameter varying multiple model adaptive estimator in order to increase its robustness and reliability with respect to different sources of model uncertainty and the disturbances that affect the UAV. Additionally, the quasi-LPV model of the UAV used in this paper has been obtained under low angle-of-attach assumption, which makes the method more suitable to be used in cruise condition. In this sense, the generalization to a more complex model which comprises the case of high angles of attack will extend the applicability of the method to other flying phases, e.g. fast altitude changes. Finally, another possible line of future research concerns the integration of the proposed method with a wind estimator.

REFERENCES

R. W. Beard and T. W. McLain. *Small Unmanned Aircraft: Theory and Practice*. Princeton University Press, Princeton, NJ, USA, 2012.

M. B. Bragg, T. Hutchinson, J. Merret, R. Oltman, and D. Pokhariyal. Effect of ice accretion on aircraft flight dynamics. In *Proceedings of the Australasian conference on robotics and automation*, 2002.

F. Caliskan and C. Hajijev. A review of in-flight detection and identification of aircraft icing and reconfigurable control. *Progress in Aerospace Sciences*, 60:12–34, 2013.

A. Cristofaro, T. A. Johansen, and A. P. Aguiar. Icing detection and identification for unmanned aerial vehicles: multiple model adaptive estimation. In *Proc. of the European Control Conference (ECC)*, pages 1651–1656, 2015.

R. W. Gent, N. P. Dart, and J. T. Cansdale. Aircraft icing. *Phil. Trans. of the Royal Soc. of London. Series A: Mathematical, Physical and Engineering Sciences*, 358:2873–2911, 2000.

S. G. Gober, G. A. Isaac, and J. W. Strapp. Characterizations of aircraft icing environments that include supercooled large drops. *Journal of Applied Meteorology*, 40(11):1984–2002, 2001.

V. Hassani, A. P. Aguiar, M. Athans, and A. M. Pascoal. Multiple model adaptive estimation and model identification using a minimum energy criterion. In *Proc. of the 26th American Control Conference (ACC)*, pages 518–523, 2009.

A. Kwiatkowski, M.-T. Boll, and H. Werner. Automated generation and assessment of affine LPV models. In *Proc. of the 45th IEEE Conference on Decision and Control (CDC)*, pages 6690–6695, 2006.

D. Rotondo, A. Cristofaro, T. A. Johansen, F. Nejjari, and V. Puig. Icing detection in unmanned aerial vehicles with longitudinal motion using an LPV unknown input observer. In *Proc. of the IEEE Multi-Conference on Systems and Control*, pages 984–989, 2015a.

D. Rotondo, A. Cristofaro, T. A. Johansen, F. Nejjari, and V. Puig. Detection of icing and actuator faults in the longitudinal dynamics of small UAVs using an LPV proportional integral unknown input observer. In *Proc. of the 3rd International Conference on Control and Fault-Tolerant Systems (SysTol)*, 2016.

D. Rotondo, V. Hassani, and A. Cristofaro. A multiple model adaptive architecture for the state estimation in discrete-time uncertain LPV systems. In *American Control Conference (ACC)*, 2017.

D. Rotondo, V. Puig, F. Nejjari, and M. Witczak. Automated generation and comparison of Takagi-Sugeno and polytopic quasi-LPV models. *Fuzzy Sets and Systems*, 277:44–64, 2015b.

M. M. Seron, T. A. Johansen, J. A. De Doná, and A. Cristofaro. Detection and estimation of icing in unmanned aerial vehicles using a bank of unknown input observers. In *Proc. of the 5th Australian Control Conference (AUCC)*, pages 87–92, 2015.

J. S. Shamma. An overview of LPV systems. In J. Mohammadpour and C. Scherer, editors, *Control of Linear Parameter Varying Systems with Applications*, pages 3–26. Springer, 2012.

D. Simon. Kalman filtering for fuzzy discrete time dynamic systems. *Applied Soft Computing*, 3:191–207, 2003.

K. L. Sørensen, M. Blanke, and T. A. Johansen. Diagnosis of wing icing through lift and drag coefficient change detection for small unmanned aircraft. In *Proc. of the 9th IFAC Symposium on Fault Detection, Supervision and Safety of Technical Processes*, pages 732–739, 2015a.

K. L. Sørensen, A. S. Helland, and T. A. Johansen. Carbon nanomaterial-based wing temperature control system for in-flight anti-icing and de-icing of unmanned aerial vehicles. In *Proc. of the IEEE Aerospace Conference*, 2015b.

X.-D. Sun and I. Postlethwaite. Affine LPV modelling and its use in gain-scheduled helicopter control. In *UKACC International Conference on Control*, pages 1504–1509, 1998.

M. Tousi and K. Khorasani. Robust observer-based fault diagnosis for an unmanned aerial vehicle. In *Proc. of the IEEE International Systems Conference (SysCon)*, pages 428–434, 2011.

A. Wenz and T. A. Johansen. Icing detection for small fixed wing UAVs using inflight aerodynamic coefficient estimation. In *Proc. of the IEEE Conference on Control Applications (CCA)*, pages 230–236, 2016.